

# EXPERIMENTAL AND NUMERICAL INVESTIGATION OF THE ELONGATIONAL VISCOSITY EFFECTS IN A COAT-HANGER DIE

*Y. Sun and M. Gupta*

*Mechanical Engineering-Engineering Mechanics Department  
Michigan Technological University, Houghton, MI 49931*

*J. Dooley, K. A. Koppi and M. A. Spalding  
The Dow Chemical Co., Midland, MI 48667*

## Abstract

The flow in a flat die is simulated using the axisymmetric and planar elongational viscosities of a low-density polyethylene (LDPE) resin. Elongational viscosity is found to have only a limited effect on the velocity distribution at the die exit. However, the predicted pressure drop in the die increased when the effect of elongational viscosity is included in the simulation. Predicted pressure drop is compared with the corresponding experimental data.

## Introduction

Many different flat die configurations, namely, a T-die, a fishtail die or a coat-hanger die, are commonly used to extrude thin sheet or film [1]. In all of these configurations polymer is fed from the extruder to the center of the die by a circular channel. Geometry of a flat die channel is designed to transform the initial circular profile into a thin rectangular cross-section of a sheet such that a uniform velocity is obtained at the die exit. The circular channel feeds the polymer to a deep transverse channel, called the manifold, which distributes the polymer across the width of the die (Fig. 1). To prevent the polymer from flowing along the die before filling the manifold, the manifold is followed by a thin slit, which is called the land. Thickness of the die channel geometry is further reduced in the die lip near the exit to obtain the required thickness of the final sheet. For the various flat die configurations listed above, the shape of the manifold is different. In the present work, a coat-hanger die was used to conduct experiments with a LDPE resin. Geometry of the die used is shown in Fig. 1. The flow of the LDPE resin in the coat-hanger die was also simulated using the PELDOM software [2]. The software simulates polymeric flows taking into account strain-rate dependence of shear as well as elongational viscosity of the polymer. Similar simulations of the flow in other flat dies has been presented in our earlier publications [3, 4], and by other research groups without including the effect of elongational viscosity on the flow [5–8]. The main objective of this paper is to compare the predictions from

numerical simulation of the flow with the corresponding experimental data.

## Material Properties

The material used for these studies was a LDPE resin with a melt index (MI) of 0.22 g/10 min (190°C, 2.16 kg) and a solid density of 0.921 g/cm<sup>3</sup>. The resin was manufactured by The Dow Chemical Company. To capture the strain-rate dependence of shear ( $\eta_s$ ) and elongational viscosities ( $\eta_e$ ) of the LDPE resin, the Carreau model [9] and Sarkar-Gupta model [10], respectively, were used in this work:

$$\eta_s = \eta_0 (1 + (\lambda_e e_{II})^2)^{\frac{n-1}{2}} \quad (1)$$

$$\eta_e = \eta_0 \left[ T_r + \delta \left\{ 1 - \frac{1}{\sqrt{1 + (\lambda_e e_{II})^2}} \right\} \right] (1 + (\lambda_2 e_{II})^2)^{\frac{m-1}{2}} \quad (2)$$

where,  $e_{II}$ , the second invariant of the strain-rate tensor is the same as the shear rate,  $\dot{\gamma}$ , for a shear flow, and  $\sqrt{3}\dot{\epsilon}$  and  $2\dot{\epsilon}$ , respectively, for axisymmetric and planar elongational flows, with  $\dot{\epsilon}$  being the elongation rate. In equations (1) and (2),  $\eta_0$ ,  $\delta$ ,  $\lambda$ ,  $\lambda_1$ ,  $\lambda_2$ ,  $n$  and  $m$  are material parameters, and  $T_r$ , the Trouton ratio at low strain rates, is 3 for an axisymmetric flow and 4 for a planar flow. An Arrhenius-type model [9] is used here for temperature dependence of the zero-shear viscosity ( $\eta_0$ ), in Eqns (1) and (2):

$$\eta_0 = A \exp(T_a / T) \quad (3)$$

where  $T$  is the temperature of the polymer, and  $A$  and  $T_a$  are material parameters. For the LDPE resin, the values of various viscosity parameters for Carreau model and the Sarkar-Gupta model are given in Table 1 [11]. Based upon these parameter values, the shear and elongational viscosities of the resin are shown in Fig. 2.

The thermal conductivity ( $K$ ), melt density ( $\rho$ ) and heat capacity ( $C_p$ ) of the polymer were assumed to be constant for the range of temperature in the flat dies.

Since the actual values of  $K$ ,  $\rho$  and  $C_p$  for the resin used in experiments were not known, typical values of  $K$ ,  $\rho$  and  $C_p$  for a LDPE resin were used for the flow simulation. These values of  $K$ ,  $\rho$  and  $C_p$  are also given in Table 1 [3, 11].

## Geometry of the Film Die

Geometry of the film die used in this work [12], is shown in Fig. 1. The polymer is fed vertically to the top of the die manifold through a cylindrical channel. The cylindrical channel has a constant diameter of 1.27 cm. The upper side of the die is completely flat. Various features such as the manifold, land and lip shown in Fig. 1 are machined in the lower die plate. Near the entrance in the middle of the die, the manifold depth and width are 0.95 and 1.27 cm, respectively. The manifold depth and width decrease towards the sides, to 0.254 and 0.254 cm, respectively, at the ends. From the die manifold, the polymer enters into a thin land. The land has a uniform depth of 0.254 cm. The larger depth of the die manifold helps to distribute the polymer across the width of the die before it enters in the thin triangular land. Length of the land along the flow direction is 5.451 cm at the two ends and 10.16 cm in the middle. Near the exit, in the lip region of the die, the depth of the die channel decreases further to 0.1524 cm. Along the flow direction, the length of the lip region as well as that of the converging transition region between the land and lip is 0.635 cm each. As shown in Fig 1, the film die has four pressure transducers, which are located in the land region. Transducers 1 and 2 are located along the center line of the die at a distance of 8.89 and 3.81 cm, respectively, from the die exit. Transducers 2, 3 and 4 are located at the same axial location, and 5.08 cm apart from each other in the lateral direction. The four transducers are connected to a data acquisition system, which records the pressure data on a computer.

## Results and Discussion

The finite element mesh used to simulate the flow in the film die is shown in Fig. 3. The finite element mesh has 252,759 tetrahedral elements. A constant velocity corresponding to the flow rate of  $2.72 \times 10^{-6} \text{ m}^3/\text{s}$  was enforced at the entrance of the circular channel. A no-slip condition was specified at the die walls, and no-traction (stress-free) condition was employed at the exit.

Fig. 4 compares the velocity distributions in the midplane of the die lip predicted by the generalized Newtonian formulation (Fig. 4 a) and that after including the effect of elongational viscosity in the simulation (Fig. 4 b). Corresponding velocity distributions in the plane of symmetry passing through the axis of the circular inlet channel are shown in Fig. 5. With the generalized

Newtonian formulation, the constant velocity distribution at the entrance of the circular channel quickly changes to the fully developed velocity profile. In order to achieve the fully developed profile, the fluid near the middle of the channel needs to accelerate, whereas the fluid near the channel walls decelerates. The elongational flow due to this redistribution of the velocity field is slowed down when the effect of higher elongational viscosity is included in the simulation. Therefore, when the effect of the higher elongational viscosity is included in the simulation (Fig. 5b), the polymer is not able to achieve a fully developed velocity profile before it reaches the die entrance.

Because of the larger depth of the manifold, instead of entering the land region of the die, polymer has a tendency to first flow through the manifold. However, since the depth and width of the manifold decrease towards the two ends, the flow in the manifold is somewhat elongational in nature. Due to this elongational nature of the flow in the manifold, as the effect of elongational viscosity is included in the simulation, the polymer has a slightly smaller tendency to flow through the manifold and higher tendency to enter the triangular land region. Therefore, near the entrance, the velocity is slightly higher in the triangular land region when the effect of elongational viscosity is included in the simulation. As shown in Fig. 6, this higher velocity near the middle of the triangular land region leads to higher unbalancing in the velocity distribution at the die exit when the effect of elongational viscosity is included in the simulation. Fig. 6 shows the exit velocity distributions at three different locations in the thickness direction. With  $h$  being the dimension of die opening in the thickness direction, and  $z$  pointing in the upward direction,  $z/h = 0$  is located at the midplane of the die, and  $z/h = 0.25$  and  $z/h = -0.25$  correspond to the centers of the upper and lower die halves, respectively, at the die exit. It is evident from Fig. 6 that the velocity in the midplane is lower when the effect of elongational viscosity is included in the simulation, whereas away from the midplane the velocity is higher with elongational viscosity effect. It was confirmed that the total flow rate at the die exit is the same for the simulations with and without elongational viscosity effect, and matches with the flow rate specified at the entrance.

Figs. 7 and 8 show the effect of elongational viscosity on the pressure distributions in the film die. Fig. 7 shows the pressure distribution in the plane passing through the middle of the die lip, whereas the pressure in the plane of symmetry through the middle of the inlet channel is shown in Fig. 8. Total pressure drop in the film die and circular inlet channel predicted by the generalized Newtonian formulation is 4.2 MPa. The inlet pressure increases to 4.8 MPa when the effect of elongational viscosity is included in the simulation. A large fraction of this increase in total pressure drop due to high elongational viscosity is in the region where the circular

channel is connected to the die inlet. In this region, where the polymer makes a 90° turn, the flow is highly elongational in nature. Additional increase in pressure drop due to high elongational viscosity of polymer occurs in the converging transition region between the die land and lip, and near the abrupt step between the manifold and land.

For the pressure transducers locations shown in Fig 1, the experimental data and the corresponding numerical predictions are given in Table 2. In general and as expected, the predicted pressure at the four transducer locations was higher when the effect of elongational viscosity was included in the simulation as compared to the pressures predicted by generalized Newtonian formulation. For all four transducer locations the predicted pressure is in excellent agreement with the experimental data. Numerical simulation predicted the highest pressure along the center line (location 2) which decreased as the distance from the center line is increased. However, the decrease in the pressure away from the centerline is within the accuracy of the experimental measurement ( $\pm 0.1$  MPa), and could not be captured in the experimental data.

### Conclusions

The axisymmetric and planar elongational viscosities of a LDPE resin were used in the present work to simulate the flow in a flat die. For the flow of LDPE resin in the flat die used, the elongational viscosity is found to affect the velocity at the die exit, as well as the predicted pressure drop in the die. Predicted pressure distribution in the die is found to be in good agreement with the corresponding experimental data.

### Acknowledgement

This work is supported by the National Science Foundation Grant DMI-0200091.

### References

1. W. Michaeli, *Extrusion Dies for Plastics and Rubber*, Hanser Publishers, New York (1992).
2. PELDOM software, Plastic Flow, LLC, 1206 Birch Street, Houghton, MI 49931.
3. Y. Sun and M. Gupta, *Int. Polym. Proc. Journal*, **18**, 356 – 361 (2003)
4. Y. Sun and M. Gupta, *SPE ANTEC Tech. Papers*, **50**, 3307 – 3311 (2004).
5. M. Gupta, Y. Jaluria, V. Sernas, M. Esseghir and T. H. Kwon, *Poly. Eng. Sci.*, **33**, 393 (1993).
6. R. Shankar and R. Ramanathan, *SPE ANTEC Tech. Papers*, **41**, 65 (1995).
7. W. A. Gifford, *SPE ANTEC Tech. Papers*, **44**, 290 (1998).
8. W. A. Gifford, *Poly. Eng. Sci.*, **41**, 1886 (2001).

9. R. B. Bird, R. C. Armstrong and O. Hassager, *Dynamics of Polymeric Liquids*, Vol. 1 and 2, Wiley, New York (1987).
10. D. Sarkar and M. Gupta, *J. Reinf. Plast. Comp.*, **20**, 1473 (2001).
11. P. Beaupre and M. Gupta, *Int. Polym. Proc. Journal*, **17**, 370 (2002).
12. J. Dooley, *SPE ANTEC Tech. Papers*, **36**, 168 (1990).

Table 1. Material properties of the LDPE resin used in this study [3, 11].

Thermal and mechanical properties	$K$	0.25 W/m K	
	$\rho$	740 kg/m <sup>3</sup>	
	$C_p$	2300 J/kg K	
Shear viscosity	$A$	469.08 Pa·s	
	$T_a$	2721.7 K	
	$\lambda$	0.6509	
	$n$	0.401	
Elongational viscosity	Planar	$\delta$	37.3
		$\lambda_1$	11.795 s
		$\lambda_2$	0.4571 s
		$m$	0.45
	Axisymmetric	$\delta$	0.0
		$\lambda_2$	0.02242 s
		$m$	0.349

Table 2 Comparison of Experimental Results and FE Simulation results: Pressure

Pressure Transducer Number	Experimental data ( $\pm 0.1$ MPa)	Numerical prediction (MPa)	
		With elongational viscosity	Without elongational viscosity
1	2.8	3.01	2.84
2	1.5	1.57	1.44
3	1.6	1.54	1.43
4	1.5	1.48	1.40

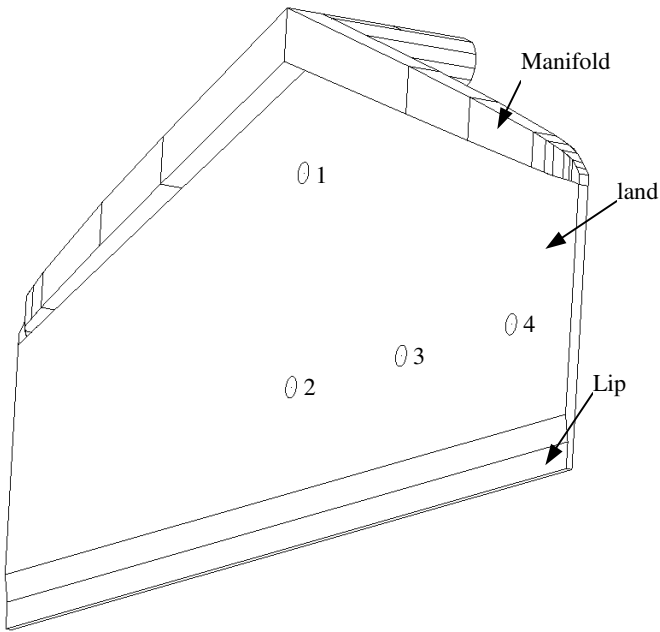


Fig. 1 Geometry of the flat die and locations of pressure transducers.

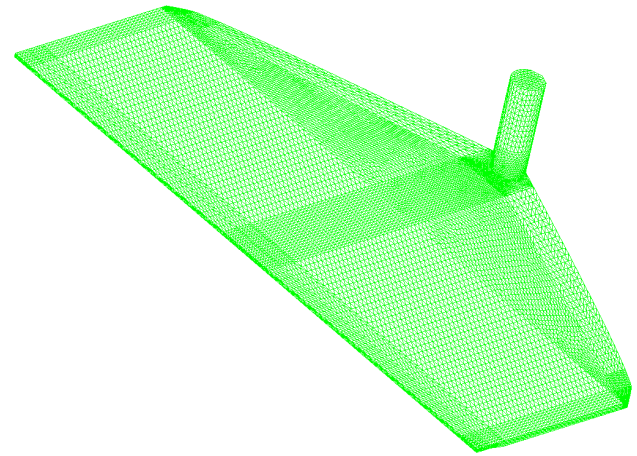


Fig. 3 Finite element mesh in the coat-hanger die.

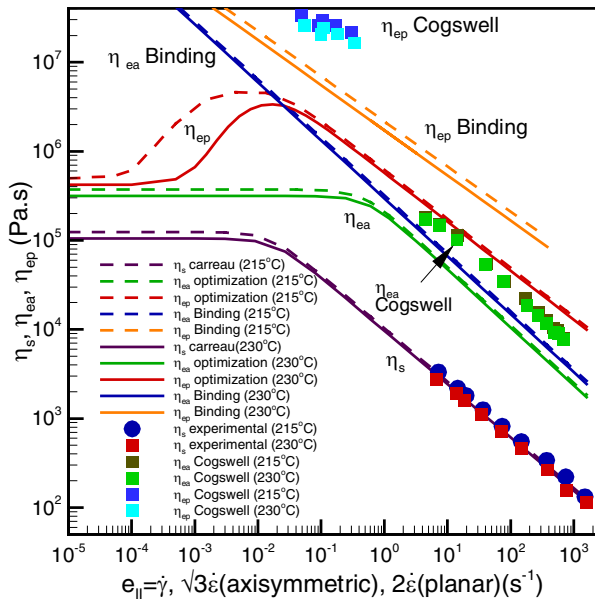


Fig. 2 Variation of shear ( $\eta_s$ ) and elongational ( $\eta_{ep}$  (planar),  $\eta_{ea}$  (axisymmetric)) viscosities of LDPE with the second invariant of strain-rate tensor ( $e_{II}$ ).

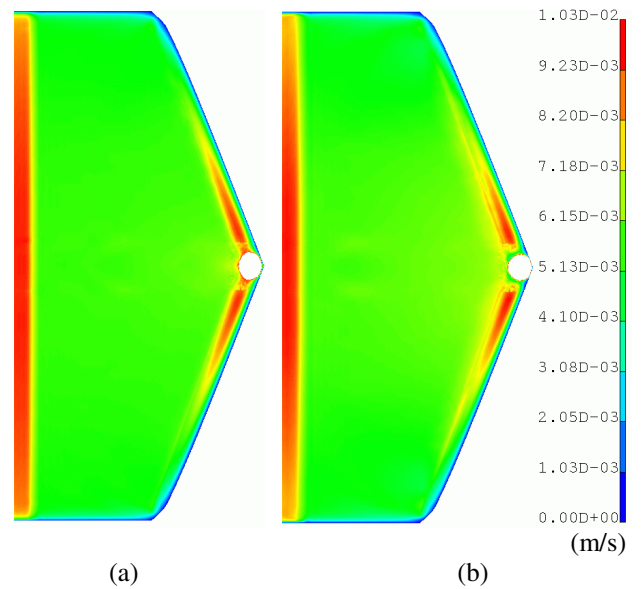


Fig. 4 Velocity distribution in the mid-plane of the flat die. (a) Carreau model, (b) Sarkar-Gupta model for elongational viscosity.

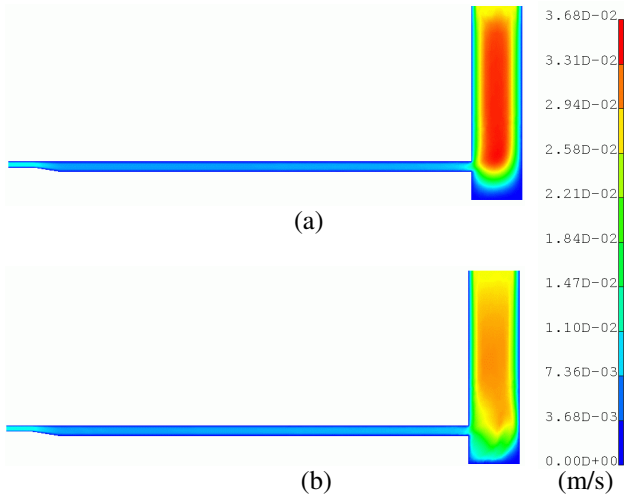


Fig. 5 Velocity distribution in the plane of symmetry in the thickness direction of the flat die. (a) Carreau model, (b) Sarkar-Gupta model for elongational viscosity.

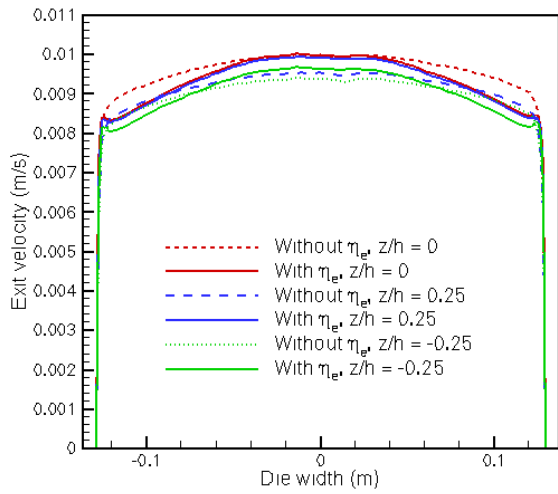


Fig. 6 Velocity distribution at the die exit.

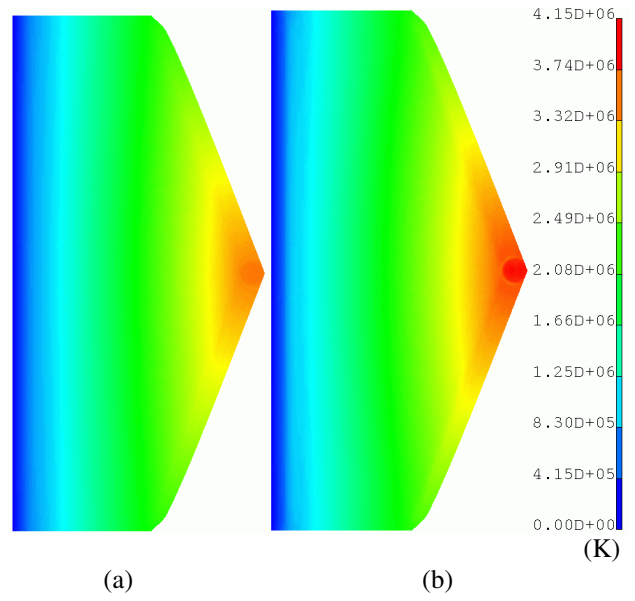


Fig. 7 Pressure distribution in the mid-plane of the flat die. (a) Carreau model, (b) Sarkar-Gupta model for elongational viscosity.

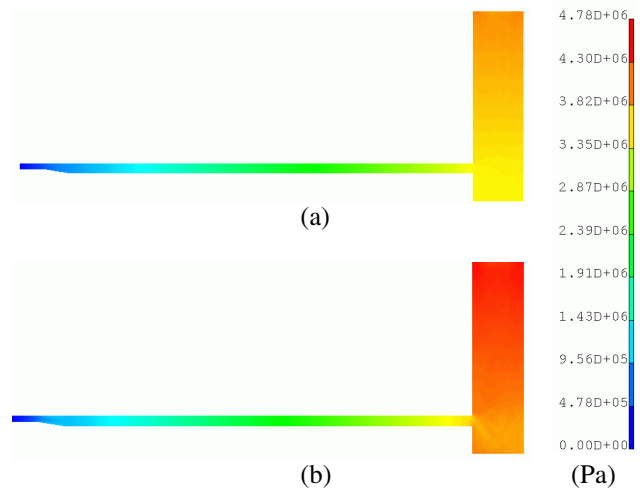


Fig. 8 Pressure distribution in the plane of symmetry in the thickness direction of the flat die. (a) Carreau model, (b) Sarkar-Gupta model for elongational viscosity.